AIAA JOURNAL
Vol. 41, No. 10, October 2003

Analysis and Experiment of Gas Leakage Through Composite Laminates for Propellant Tanks

Hisashi Kumazawa*
National Aerospace Laboratory, Tokyo 181-0015, Japan
Takahira Aoki†
University of Tokyo, Tokyo 113-8656, Japan
and
Ippei Susuki‡
National Aerospace Laboratory, Tokyo 181-0015, Japan

The mechanism of the through-thickness gas leakage of carbon fiber-reinforced plastics (CFRP) laminates is investigated in view of propellant leaks for composite tanks of reusable launch vehicles. In this study analysis of leakage caused by the existence of matrix cracks acting as the chain of leakage paths is developed under the simple assumption that conductance for leakage is a function of crack-opening displacements. The analytical results in consideration of mechanical and thermal loads are compared with experimental results, which are measured as helium gas leaks through carbon fiber-reinforced plastics laminates containing matrix cracks at room temperature. Good agreement between the analytical and experimental data is confirmed. Numerical analysis based on the proposed method can be used to evaluate the influence of mechanical loads on propellant leak through CFRP cross-ply laminates. The analytical calculations show that the increase of propellant leakage can be caused by the enlargement of crack-opening displacements caused by mechanical and thermal loads, increase of crack density, and decrease of temperature.

I. Introduction

CARBON-FIBER-REINFORCED-PLASTICS (CFRP) tanks are expected to be utilized in several fields for the advantage of reduced weight. For reusable launch vehicles, particularly single-stage launchers, weight reduction of propellant tanks, which represent a large part of the structural mass, are of high priority and can be attained with the use of CFRP composites. Recent studies[1,2] pointed out that the cryogenic temperature of liquid hydrogen affects the properties of CFRP materials and induces severe thermal strains. One of the major consequences is the initiation of matrix cracks at relatively low loads even in the toughened CFRP laminates. The accumulation of matrix cracks not only influences mechanical performance of the structures but can also lead to propellant leakage through the laminate tank walls.[3] Other experimental studies revealed that the existence of matrix cracks in the CFRP laminate could cause large leak rate compared to the permeation caused by diffusion.[4–7] However, analytical investigations of leakage for these CFRP laminates have not yet been pursued.

The objective of this study is to clarify the mechanism of the through-thickness propellant leakage of CFRP cross-ply laminates caused by the existence of chains of matrix cracks. In this study the leakage through CFRP laminates is experimentally investigated with the use of small test specimens instead of costly full- or subscale tanks. An analytical formulation is developed based on the simple modeling that there is a relationship between leakage and opening displacements of matrix cracks. Leak experiments using cruciform laminate specimens are conducted to acquire experimental data. Constants used in the leakage analysis are determined by the experimental results under uniaxial loadings, and then leak rates under biaxial loadings are calculated with these constants and compared with the experimental results. The comparison shows that the numerical calculations are in good agreement with the experimental results, and crack-opening displacements have close relationship with leakage. The leak analysis is proved to be capable of calculating the leak behavior under mechanical loading including biaxial tension. In addition, the influences of matrix crack density and temperature on leakage are numerically evaluated based on the leak analysis.

Received 17 September 2002; revision received 12 May 2003; accepted for publication 21 May 2003.

*Researcher, Structures and Material Research Center, 6-13-1 Ohsawa, Mitaka-shi. Member AIAA.
†Associate Professor, Department of Aeronautics and Astronautics, 7-3-1 Hongo, Bunkyo-ku. Member AIAA.
‡Group Leader, Structures and Material Research Center, 6-13-1 Ohsawa, Mitaka-shi.

II. Leak Analysis

The gas permeation through a laminate is composed of two mechanisms: diffusion and leak. Gas diffusion is the phenomenon that takes place when the gas atoms diffuse into the materials and pass through the laminate. In the case of leakage, gas flows through the leak path that consists of continuously connected matrix cracks in each layer, which result in a sequence of connecting passages between both sides of the laminate. If there are layers without cracks in the laminate, leakage does not take place, and diffusion alone can be present. Generally, the permeation caused by diffusion is negligible compared to that caused by leakage through leak paths.[4] The analytical scheme presented here is based on the assumption of leakage from one side of the laminate surface to the other, through the cascade of matrix cracks developed in each ply of the laminate.

A. Modeling

In this model it is postulated that cracks exist in each component ply of the laminate and that these cracks act as leak paths connecting both sides of the laminate. Therefore, the basic assumption for leakage is that the leak rate Q is governed by the overall conductance that can be derived from the combination of the multiple cracks in the laminate. The flow rate is expressed in terms of the overall conductance C and the pressure difference ΔP between the two laminate surfaces that represents the driving force of the leakage, and thus Q is in the form[8]

$$Q = C\Delta P \tag{1}$$

In the case of compressible gas, the volumetric flow rate does not represent the quantity of gas flow unless the pressure and temperature are specified. In vacuum engineering leak rate Q (Pa m^3/s) for compressible gas in Eq. (1) is expressed as the product of volumetric flow rate Q_V (m^3/s) and pressure P (Pa) at specified temperature:

$$Q = P \cdot Q_V \tag{2}$$

The mass-flow rate can be recalculated from leak rate using Eq. (A6) in Appendix A.

The overall through-the-thickness conductance C is derived from the combined sum of intraply conductances through matrix cracks and interply conductances at each crack intersection between two matrix cracks in adjacent layers. Based on the strictly theoretical crack model, the two adjacent cracks at an intersection have no overlapping area. However, the microscopic interface defects at an overlapping region of two matrix cracks in adjacent layers are assumed to provide the connecting path between the matrix cracks, as shown in Fig. 1. The matrix crack intersection point and its surrounding area of the matrix cracks in the interlaminar regions are assumed to play a major role in affecting the leakage level, acting as the throats in the leakage path. The rest of the portions of the opened cracks, including the just-mentioned intraply path, have relatively little effect on the leak rate of the entire laminate, and thus their effects on leakage are neglected herein.

Following the theory of vacuum engineering for molecular flow, conductance through an orifice is proportional to the orifice area A_{orifice} and rms velocity of molecules $\sqrt{(3RT/M)}$, where R is the gas constant, T is the absolute gas temperature, and M is the molecular weight. The orifice conductance c_{orifice} can be expressed as follows:

$$c_{\text{orifice}} \propto A_{\text{orifice}} \sqrt{T/M} \tag{3}$$

Crack openings adjacent to an intersection would widen the throat area. It is assumed that the throat at a crack intersection performs as an orifice, and the throat area is proportional to the product of crack opening displacements in adjacent layers. Thus the throat area A_k at the intersection of cracks between kth layer and $(k+1)$th layer in the cross-ply laminate (Fig. 2) is described as

$$A_k \propto \bar{\Delta}_k \bar{\Delta}_{k+1} \tag{4}$$

where $\bar{\Delta}_k$ is a mean opening displacement of cracks in kth layer. The conductance through the throat area A_k at a crack intersection is derived from Eqs. (3) and (4) as follows:

$$c_k = \Omega_M(T) \bar{\Delta}_k \bar{\Delta}_{k+1} \tag{5}$$

$$\Omega_M(T) = \Omega \sqrt{(T/T_{\text{R.T.}})(M_{\text{helium}}/M)} \tag{6}$$

where $\Omega_M\ (T)$ is the proportionality factor for an operating gas with molecular weight M at specified temperature T, $T_{\text{R.T.}}$ is the room temperature, M_{helium} is the molecular weight of helium, and Ω is the proportionality factor for helium gas at room temperature $[=\Omega_{\text{Mhelium}}(T_{\text{R.T.}})]$. Constant Ω is generally dependent on thickness of layers and shape of interface defects at the intersection of matrix cracks. Constant Ω for helium gas at room temperature is experimentally determined in the present study. Ω is assumed to be a constant throughout the laminate in consideration for approximation to avoid a complex formulation.

The number of intersection points between kth and $(k+1)$th layers in a unit area is $d_k d_{k+1}$, where d_k is a crack density of kth layer. Conductance between kth and $(k+1)$th layers per unit area $\bar{c}_k$ is thus written with c_k as

$$\bar{c}_k = d_k d_{k+1} c_k \tag{7}$$

Using reciprocal formula for series conductance, conductance through the whole laminate C is obtained as

$$C = \left(\sum_k \frac{1}{\bar{c}_k} \right)^{-1} \tag{8}$$

The conductance and the leak rate through the whole laminate are derived from Eqs. (1) and (5–8) as follows:

$$C = \Omega \sqrt{\frac{T}{T_{\text{R.T.}}} \frac{M_{\text{helium}}}{M}} \left(\sum_k \frac{1}{d_k d_{k+1} \bar{\Delta}_k \bar{\Delta}_{k+1}} \right)^{-1} \tag{9}$$

$$Q = \Omega \sqrt{\frac{T}{T_{\text{R.T.}}} \frac{M_{\text{helium}}}{M}} \left(\sum_k \frac{1}{d_k d_{k+1} \bar{\Delta}_k \bar{\Delta}_{k+1}} \right)^{-1} \Delta P \tag{10}$$

Leak rate Q is obtained as a function of crack densities, opening displacements of matrix cracks, and pressure difference. In this study matrix crack densities are enumerated from ultrasonic C-scan. The conventional two-dimensional shear-lag analysis for the cross-ply laminate (Appendix B) is applied to the calculation of mean crack-opening displacements $\bar{\Delta}_k$, which are dependent on mechanical strains caused by applied load and thermal strains caused by

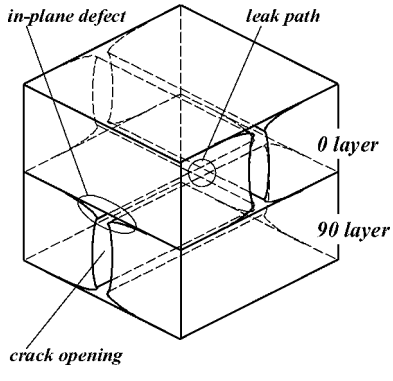

Fig. 1 Leak path at intersection of two matrix cracks.

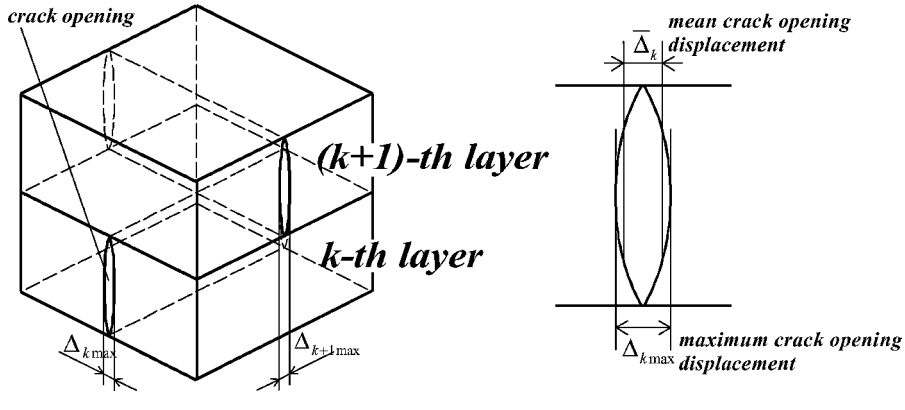

Fig. 2 Intersection of two matrix cracks and crack-opening displacements.

a decrease in temperature from the initial stress-free temperature. Knowing the initial stress-free temperature and assuming a constant Ω are important in calculating the leak rate because initial temperature is one of the determining factors for calculation of the crack-opening displacement. Initial stress-free temperature of CFRP laminates is not exactly equal to the curing temperature because of the existence of stress relaxation, and it is therefore difficult to determine the initial temperature appropriately. In the present study constant Ω and initial temperature are determined based on the experimental leak data.

B. Influences of Constant Ω and Initial Stress-Free Temperature

Leak rate in Eq. (10) is dominantly characterized by constant Ω and analytically calculated crack-opening displacement $\bar{\Delta}_k$ in each layer, which is a function of thermal strains and applied stresses [Eq. (B9) in Appendix B]. Constant Ω and initial stress-free temperature denoted as T_0 make different contributions to the calculation of leak rate. The calculated result under the range of Ω and T_0 is illustrated by the following examples. In these examples crack density is assumed to be constant regardless of temperature and stress for apparent characterization of these constants, and mean crack-opening displacement $\bar{\Delta}_k$ in the case that coefficient of thermal expansion remains unchanged irrespective of temperature is expressed as Eq. (B10) in Appendix B. Leak rates are normalized as the values under unit volume at atmospheric pressure and room temperature per unit second from Eq. (10) and Eq. (A7) in Appendix A as follows:

$$Q_{V,\mathrm{RT,ATM}} = \Omega\sqrt{\frac{T_{\mathrm{R.T.}}}{T}\frac{M_{\mathrm{helium}}}{M}}\left(\sum_k \frac{1}{d_k d_{k+1}\bar{\Delta}_k\bar{\Delta}_{k+1}}\right)^{-1}\frac{\Delta P}{P_{\mathrm{ATM}}} \tag{11}$$

Leak rates calculated as functions of temperature under the conditions of fixing one of the parameters T_0 or Ω are shown in Fig. 3a and 3b. Figure 3 shows that leak rate increases as temperature lowers mainly because of the enlarged crack-opening displacements caused by the increased thermal contraction. Moreover, coefficient $1/\sqrt{T}$ in Eq. (11) adds to the leak-rate increase at lower temperature. The decrease in temperature has the effect of increasing the leak rate. Figure 3a indicates the effect of Ω, in which the leak-rate curve is magnified proportionally at each temperature. The effect of T_0 shown in Fig. 3b is represented by the shift of the leak-rate curve parallel to temperature because leak rates are functions of temperature difference $(T - T_0)$ because the mean crack-opening displacement $\bar{\Delta}_k$ in Eq. (B10) is a linear function of temperature difference.

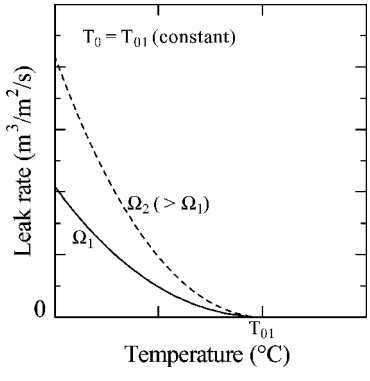

a) T_0 = constant

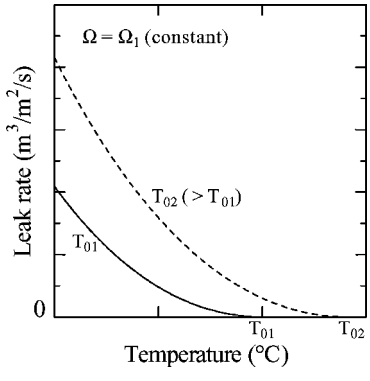

b) Ω = constant

Fig. 3 Effects of constants Ω and T_0 on leak rate under varying temperature without loading.

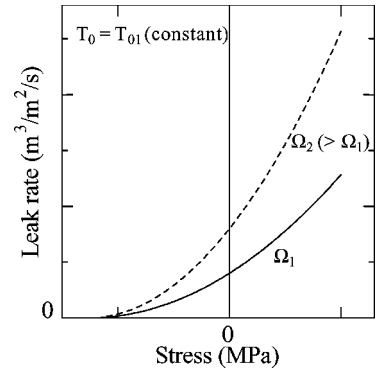

a) T_0 = constant

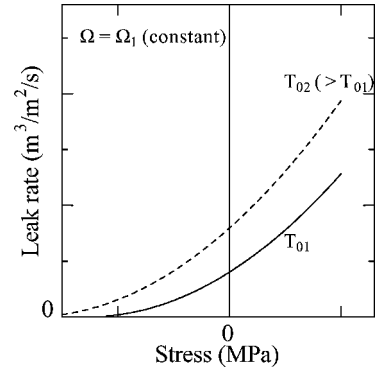

b) Ω = constant

Fig. 4 Effects of constants Ω and T_0 on leak rate under varying stress.

Figure 4 indicates the effects of Ω and T_0 on leak rate at specified temperatures under compressive and tensile stresses for the case of uniform biaxial stresses $\sigma_X = \sigma_Y$. In this paper x and y axes coincide with 0- and 90-deg directions of laminates respectively, and z axis is the direction of the ply thickness. In Fig. 4 closure of matrix cracks caused by compressive stress leads to a decrease of leak rate, and vice versa. In Fig. 4a Ω magnifies the leak rate proportionally as in Fig. 3a, and leak rates calculated with different Ω_1 and Ω_2 vanish at the same compressive stress because the crack-opening displacement $\bar{\Delta}_k$ in Eq. (11) vanishes at given stress irrespective of the value of Ω. The crack-opening displacement $\bar{\Delta}_k$ [Eq. (B10)] is a function of mechanical stress and thermal stress, and if initial temperature T_0 increases thermal stress gets larger and shifts the leak-rate curve parallel to the stress axis as shown in Fig. 4b.

Calculated leak rates under given stress and temperature increase in either case when Ω or T_0 increases, and constants Ω and T_0 cannot be determined by measured leak rate under a single condition of specific stress and temperature. It is requisite for determination of constants Ω and T_0 to acquire leak rates varying in association with temperature or stress. For example, the way to determine constants Ω and T_0 on the basis of leak rates measured as functions of stress at room temperature is outlined next. Crack-opening displacement in Eq. (B9) and leak rate in Eq. (10) are functions of biaxial stresses σ_X and σ_Y at room temperature, and rewritten as $\bar{\Delta}_k(\sigma_X, \sigma_Y)$ and

$$Q(\sigma_x, \sigma_x) = \Omega\sqrt{\frac{M_{\mathrm{helium}}}{M}}\left[\sum_k \frac{1}{d_k d_{k+1}\bar{\Delta}_k(\sigma_x,\sigma_x)\bar{\Delta}_{k+1}(\sigma_x,\sigma_x)}\right]^{-1}\Delta P \tag{12}$$

From Eq. (12), $Q(\sigma_X, \sigma_Y)/Q(0, 0)$ is independent of constant Ω as follows:

$$\frac{Q(\sigma_X, \sigma_Y)}{Q(0, 0)} = \frac{\sum_k [1/d_k d_{k+1} \bar{\Delta}_k(0, 0) \bar{\Delta}_{k+1}(0, 0)]}{\sum_k [1/d_k d_{k+1} \bar{\Delta}_k(\sigma_X, \sigma_Y) \bar{\Delta}_{k+1}(\sigma_X, \sigma_Y)]} \tag{13}$$

Measured leak rate divided by that with stress free is compared with $Q(\sigma_X, \sigma_Y)/Q(0, 0)$ calculated for several tentative initial temperatures on a graph, and suited value for T_0 can be determined to adjust the shape of the $Q(\sigma_X, \sigma_Y)/Q(0, 0)$ curve to measured data. Subsequently, Ω are resolved to quantitatively match $Q(0, 0)$ under already determined initial temperature T_0 to measured leak rate without loading.

III. Leak Experiment

A. Leak Experiment Using Cruciform Specimen

CFRP laminate cruciform specimens were biaxially loaded, and the corresponding helium leak rates were measured. Two stainless-steel cups were padded to both surfaces of the central portion of the laminate specimen as shown in Fig. 5. One of the cups supplied the helium gas (GHe) to the laminate surface, whereas the other was used to trap the leaked gas. Helium gas is poured in the supply cup from an inlet and released to the atmosphere, and flow rate of the helium gas through the supplying cup was kept low enough to introduce atmospheric pressure into the cup. The helium leak detector connected to the detection cup draws vacuum inside it, and the vacuum level is below minimum detectable pressure (1 Pa). The pressure difference between both sides of the laminate is thus controlled to be atmospheric pressure (1.0×10^5 Pa). CFRP specimens padded with these cups were biaxially loaded as shown in Fig. 6, and leak rates were measured as a function of loads and their biaxial ratios.

B. Specimen and Damage

The material systems used in this study were carbon fiber/180°C cured epoxy IM600/#133(Tg = 175°C) and IM600/#101(Tg = 252°C). The laminates with stacking sequence of $(0/0/90/90)_S$ were fabricated as the cruciform specimens glass fiber-reinforced plastics (GFRP) tabs were bonded on the laminate, and the geometry of cruciform specimens for leak test is shown in Fig. 7. IM600/#133 and IM600/#101 specimens were labeled as specimen A and specimen B, respectively. The effect of material system on the constant Ω can also be acquired by comparing the results for the different materials. The thickness of the leak test area of the specimens was about 1.2 mm. Applied loads to the cruciform specimen in the x (0 deg) and y (90 deg) directions are defined as Fx and Fy.

The strains under applied biaxial loads were measured with strain gauges to obtain the relationships between biaxial loads and strains in the strain range of 0.2%, in which no damage occurred in gauge area of the cruciform specimen. The strain gauges were detached from the cruciform specimen after the strain measurements. The specimens were applied to static biaxial tensile test for observation of damage developments and leak test under biaxial loading after the strain measurements. The strains during these tests were calculated based on the relationships between biaxial loads and strains obtained earlier.

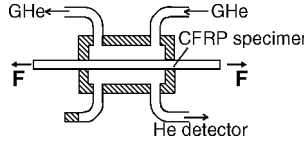

Fig. 5 Schematic view of apparatus for leak-rate measurement.

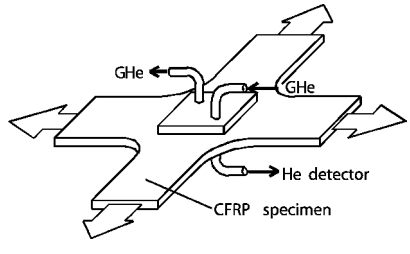

Fig. 6 Leak experiment through a laminate under biaxial loading.

Table 1 Applied loads and strains to specimen A before leak test

Cycle	Fxmax, kN	Fymax, kN	εx max, %	εx max, %	Load speed: Fx, kN/min	Load speed: Fy, kN/min
1	79.9	38.1	0.61	0.18	75.0	35.8
2	50	100	0.24	0.76	37.5	75.0

Table 2 Applied loads and strains to specimen B before leak test

Cycle	Fxmax, kN	Fymax, kN	εx max, %	εx max, %	Load speed:Fx, kN/min	Load speed:Fy, kN/min
1	62	32	0.47	0.16	75.0	38.7
2	30.4	60.4	0.15	0.46	37.7	75.0
3	40	77	0.20	0.58	39.0	75.0
4	40.2	80.5	0.19	0.61	37.5	75.0

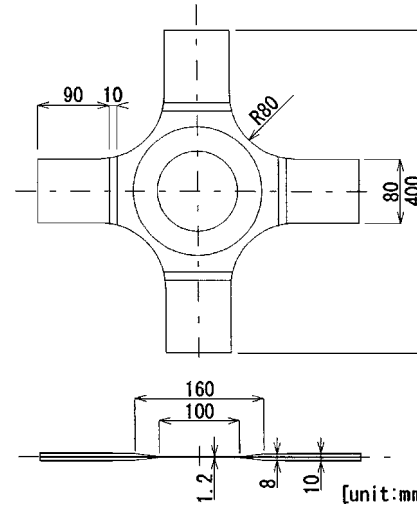

Fig. 7 Cruciform specimen for leak test.

Prior to leak experiments, two specimens were subjected to biaxial loads for several cycles to induce matrix cracks at room temperature as shown in Tables 1 and 2. The cracks in the laminate were inspected using ultrasonic with 25-MHz transducer. C-scan was obtained using a through transmission with glass reflector plate. Ultrasonic inspections from both sides, right side and backside, of a specimen were conducted to ascertain whether the crack in the 0-deg direction appeared on C-scan is in the right side or backside 0_2-deg layer. The cracks in the 0_2-deg layer on under surface appear sharper than those on the top surface because of dead band on the front face. The result of ultrasonic C-scan to observe matrix cracks in other laminate was compared with that of X-ray photography for the confirmation and proved to be in good agreement. The matrix cracks in the leak test area (45×45 mm) of the two specimens were thus inspected, as shown in Fig. 8. Figure 8 also indicates that matrix cracks exist in 90_4-deg layers and 0_2-deg layer on both sides of $(0/0/90/90)_S$ laminates after loading. The continuous series of these matrix cracks through all layers provoke the leak path through the laminate. Matrix crack densities of the laminates were enumerated from Fig. 8 and used to calculate leak rates in the leak analysis.

IV. Results and Discussion

The numerical and experimental results are compared for assessment of the validity of the leak analysis developed in the present study. The leak analysis requires the determination of an appropriate constants Ω and T_0. Hence the verification sequence starts with determination of the constants according to measured leak data of

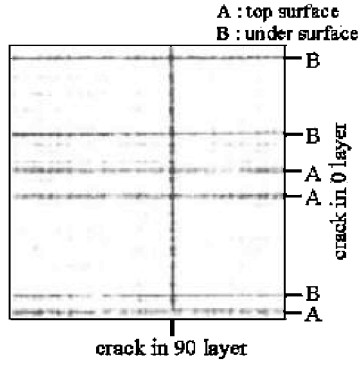

a) Specimen A (IM600/#133)

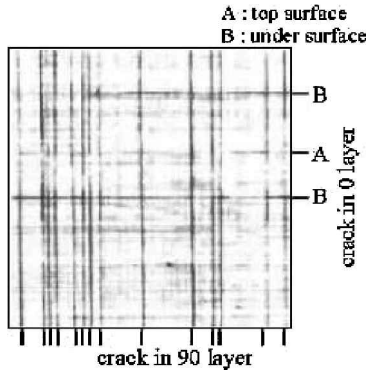

b) Specimen B (IM600/#101)

Fig. 8 Matrix crack accumulation in leak-test area (45 × 45 mm) of $(0/0/90/90)_S$ laminates.

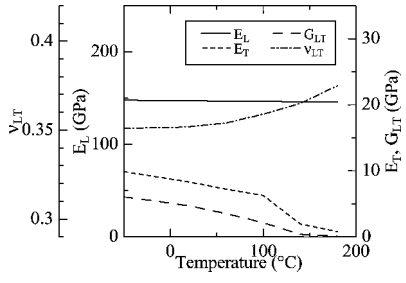

a) Elastic constants

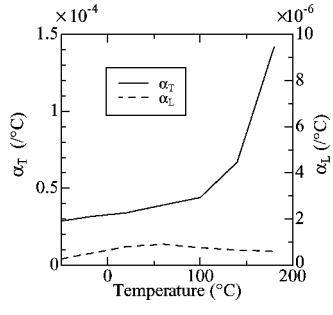

b) Thermal expansion coefficients

Fig. 9 Temperature-dependent material constants of CF/epoxy.

cruciform laminates under uniaxial load for each material. Then leak rate through the laminate under biaxial load is calculated by the leak analysis with thus determined Ω and T_0 and compared with measured leak rate. In the calculation of leak rate, the anisotropic elastic constants and thermal expansion coefficients of IM600/#133 are treated as dependent on temperature as presented in Fig. 9 (Ref. 1). In the results leak rates are converted to the values under unit volume at atmospheric pressure and room temperature per second through the use of Eq. (A7) in Appendix A.

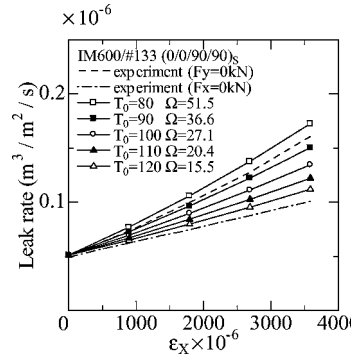

Fig. 10 Comparison between measured and analytical leak rates under uniaxial load (specimen A).

A. Comparison Between Leak Analysis and Experiment

The method to determine constants Ω and T_0 with Eq. (13) is applied, and the comparison between numerical and experimental results is shown in Fig. 10. Leak rates are calculated numerically with varying initial temperatures. Leak rates through the cruciform laminate under uniaxial load are experimentally measured at room temperature. Numerical calculation of the leak rate is conducted with initial temperature T_0 from 80 to 120°C at 10°C intervals, and constant Ω for each initial temperature that is determined by comparing the calculated leak rate and corresponding measured value under zero mechanical loads ($\varepsilon x = 0$). Though numerical results under uniaxial load do not vary with respect to the direction of the uniaxial loading, experimental results show different measured leak rates under different loading direction (Fig. 10). For the symmetric property of the stacking sequence $(0/0/90/90)_S$ and boundary conditions on the middle surface and the external surface, the mean opening displacements of cracks in 0_2-deg and 90_4-deg layers under biaxial stresses, $\bar{\Delta}_0(\sigma_X, \sigma_Y)$ and $\bar{\Delta}_{90}(\sigma_X, \sigma_Y)$, have the relationship as follows [Eq. (B11) in Appendix B]:

$$\bar{\Delta}_0(\sigma_1, \sigma_2) = \bar{\Delta}_{90}(\sigma_2, \sigma_1) \tag{14}$$

and $\bar{\Delta}_0(\sigma_X, \sigma_Y) \times \bar{\Delta}_{90}(\sigma_X, \sigma_Y)$ is identical under the two conditions $(\sigma_X, \sigma_Y) = (\sigma_1, \sigma_2)$ and (σ_2, σ_1) derived from Eq. (14) as follows:

$$\bar{\Delta}_0(\sigma_1, \sigma_2) \times \bar{\Delta}_{90}(\sigma_1, \sigma_2) = \bar{\Delta}_0(\sigma_2, \sigma_1) \times \bar{\Delta}_{90}(\sigma_2, \sigma_1) \tag{15}$$

Thus the calculated leak rate $Q(\sigma_X, \sigma_Y)$ in Eq. (12), which is a function of $\bar{\Delta}_0(\sigma_X, \sigma_Y) \times \bar{\Delta}_{90}(\sigma_X, \sigma_Y)$, has no difference irrespective of load direction from Eq. (15):

$$Q(\sigma_1, \sigma_2) = Q(\sigma_2, \sigma_1) \tag{16}$$

Under the present assumption of leakage model, the leak analysis has been developed with neglecting the intraply conductance through the cracks in 90_4-deg layer, which is a function of $\bar{\Delta}_{90}(\sigma_X, \sigma_Y)$. In the experimental results change in the intraply conductance through matrix cracks in 90_4-deg layer could have led to the difference between two measured leak rates under different load directions as

$$Q(\sigma_1, \sigma_2) \neq Q(\sigma_2, \sigma_1) \tag{17}$$

It is unachievable for the leak analysis for $(0/0/90/90)_S$ laminates under the present assumption to obtain the numerical results dependent on the direction of uniaxial load. Thus the constants are determined to accommodate the calculated leak rate with the least difference from two experimental results for different load directions concurrently.

Suitable constants are selected for the leak-rate curve lying between the measured leak rates under uniaxial load in the x (0-deg) direction and y (90-deg) direction. Figure 10 indicates that the calculated leak rates under condition of initial temperatures ranging from 90 to 110°C are approximately suitable for the measured leak rates through the laminate specimen A submitted to uniaxial load. Ω ranges from 20.4 to 36.6 $m^3/m^2/s$ with temperature from 90 to 110°C. Though value of Ω is responsive to small change of initial temperature, $T_0 = 100$°C and $\Omega = 27.1$ $m^3/m^2/s$ are used as representative values in the calculation for leak rate. In a similar way

Table 3 Constants Ω and T_0 for $(0/0/90/90)_S$ laminates

Specimen	Material	Ω, $m^3/m^2/s$	T_0, °C
A	IM600/#133	27.1	100
B	IM600/#101	43.6	100

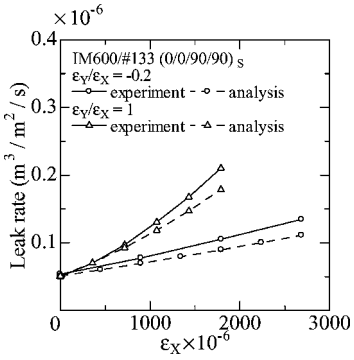

a) Specimen A (IM600/#133)

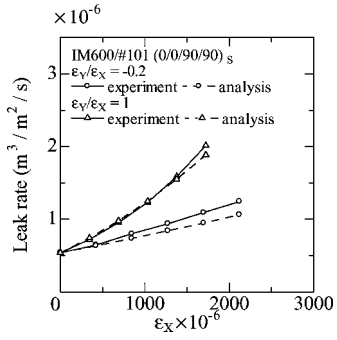

b) Specimen B (IM600/#101)

Fig. 11 Comparison between measured and analytical leak rates through $(0/0/90/90)_S$ laminate.

the constant Ω for specimen B was determined as a representative value by comparing calculated leak rates with experimental results as shown in Table 3. In this determination procedure material properties of IM600/#101 are assumed to be identical to those of IM600/#133 because the two CFRP materials consist of 180°C cured epoxy resin and identical carbon fiber, both of which dominantly determine the material constants.

Table 3 reveals that the constant Ω for specimen A is lower compared to that for specimen B. Constant Ω in Eqs. (5) and (6), which indicates the likelihood of gas passage at the crack intersection, can easily be surmised to be affected by the extent of interface damage at an overlapping region of cracks. It can be deduced that Ω for specimen A is lower than that of specimen B because the microscopic delamination at the crack intersection in toughened material specimen A would be smaller than that in specimen B. The difference of damage level might also have been caused by the conditions of loading. Strain-free initial temperature is not necessarily equal to curing temperature, but seems to be much lower than the latter. The 4-mm GFRP tabs were bonded to the 1.2-mm-thick laminate specimens on both side with thermosetting adhesive films as shown in Fig. 7. Fall in temperature from curing temperature of adhesive films (120°C) supposedly induces compression in the gauge area of specimens caused by large thermal contraction of the GFRP tabs compared to that of the CFRP gauge area at room temperature.

Numerical calculations for the two CFRP laminates, of which matrix crack densities are different as shown in Fig. 8, are compared with experimental results in Fig. 11. This figure shows the measured leak rates of specimen A and specimen B under biaxial load ratios $Fy/Fx = 1$ ($\varepsilon y/\varepsilon x = 1$) and $Fy/Fx = 0$ ($\varepsilon y/\varepsilon x = -0.2$), together with the numerical results using Ω determined from uniaxial load test. The numerical calculations are in very good correlation with the experimental results in Fig. 11. The leak rate through the laminate in the case of a biaxial strain ratio $\varepsilon y/\varepsilon x = 1$ is larger than that in case of strain ratio $\varepsilon y/\varepsilon x = -0.2$. This enhancement of leakage implies that the amount of crack-opening displacements under strain ratio $\varepsilon y/\varepsilon x = 1$ are larger than those under strain ratio $\varepsilon y/\varepsilon x = -0.2$, and in consequence conductance of leak path composed of cracks becomes relatively higher. Figure 11 indicates that the biaxial stress level and its ratio have a great impact on the leak rates.

B. Numerical Examples

Leak rates are numerically calculated by Eq. (11) to clarify the effect of crack density, biaxial stresses, and temperature on leakage for the IM600/#133 $(0/0/90/90)_S$ laminates. The constant $\Omega = 27\ m^3/m^2/s$ and initial temperature $T_0 = 100°C$ are assumed in the subsequent calculations.

Leakage through the laminate with no mechanical load at room temperature as function of crack density is shown in Fig. 12. In this figure matrix crack densities in the 0_2-deg and 90_4-deg layers (d_0 and d_{90}) are assumed to be equal. Leak-rate increases in accordance with increasing amounts of matrix cracks because parallel leak paths grow in number.

The effect of crack density and stress on the leak rate is shown in Fig. 13. In this figure the leak rates are calculated under the condition of crack density $d_0 (= d_{90}) = 0.5, 1.0$/cm and stress ratio of $\sigma_Y/\sigma_X = 0, 1$ at room temperature for illustration. Figure 13 shows that not only the crack density but also the load levels and their ratio

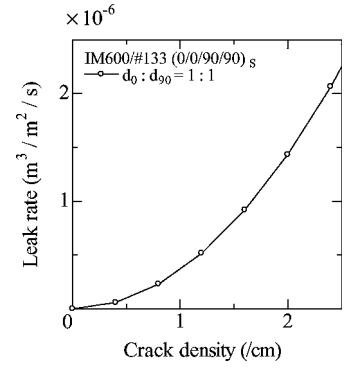

Fig. 12 Relationships between calculated leak rate and crack density through IM600/#133 $(0/0/90/90)_S$ laminate with no mechanical load.

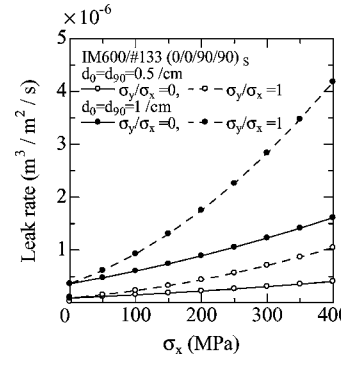

Fig. 13 Increase of calculated leak rate through IM600/#133 $(0/0/90/90)_S$ laminate under biaxial stresses.

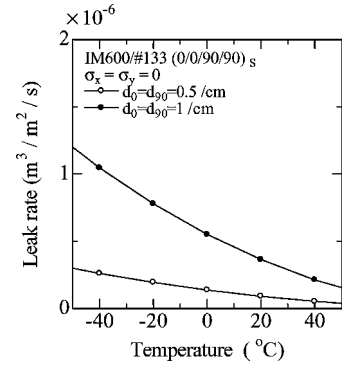

Fig. 14 Relationships between temperature and calculated leak rate through IM600/#133 $(0/0/90/90)_S$ laminate with no mechanical load.

affect the leakage. The leak rate under biaxial stresses $\sigma_Y/\sigma_X = 1$ is larger than that under uniaxial stress $\sigma_Y/\sigma_X = 0$ as a result of the difference in crack-opening displacements.

Leak rate as function of temperature under no mechanical load is calculated and shown in Fig. 14. Crack densities d_0 and d_{90} are assumed to remain unchanged as the temperature is lowered. The decrease of temperature results in the increase of leak rate, which is caused by the enlargement of crack-opening displacements caused by the thermal contraction and the temperature effect on velocity and density of molecules.

V. Conclusions

To clarify the mechanism of propellant leakage through damaged carbon fiber-reinforced plastics cross-ply laminates, leak analysis based on the opening displacements of matrix cracks has been developed. In leak analysis conductance at the crack intersection in the laminate acting as a throat of the leak path is assumed to be proportional to the product of opening displacements of matrix cracks in adjacent layers, based on the analogy with the molecular flow through an orifice. Permeability of the whole laminate has been derived from the combined sum of the conductance at the intersection of matrix cracks, and numerical calculations are in good agreement with experimental results, which have been acquired from the leak tests through laminates with matrix cracks at room temperature. The leak analysis in this study is based on a simple assumption of a relationship between conductance and crack opening and can be used to evaluate the influence of mechanical and thermal loads on propellant leak through carbon fiber-reinforced plastics cross-ply laminates. The results of this study also indicate that the leak characteristics at the intersection of matrix cracks would depend on the expansion of the microscopic defects in the vicinity of the crack intersections, and the enlargement of crack opening displacements as a result of mechanical and thermal loads has a great impact on the gas leakage.

Appendix A : Unit Conversion for Leak Rate

The ideal gas law is written as follows[8]:

$$P = nkT \tag{A1}$$

$$n = N/V \tag{A2}$$

$$k = mR/M \tag{A3}$$

where P is the pressure, n the concentration of molecules, k the Boltzmann's constant, T the absolute temperature, N the number of molecules, V the volume, m the mass of a molecule, R the gas constant, and M the gram molecular weight.

The ideal gas law is rewritten from Eqs. (A1–A3) as follows:

$$PV/T = (w/M)R = \text{const} \tag{A4}$$

where w is the weight of gas(= mN). The relationship between volumetric flow rate Q_V (m^3/s) and mass-flow rate Q_W (g/s) is obtained from Eq. (A4) as follows:

$$PQ_V/T = (Q_W/M)R \tag{A5}$$

Mass-flow rate Q_W (g/s) is obtained using R (Pa m^3/g mole K), $T(K)$, and M (g/mole) from Eqs. (2) and (A5) as

$$Q_W = Q \cdot M/RT \tag{A6}$$

Leak rates in the analysis and experiment in this paper are converted to the value under unit volume at atmospheric pressure and room temperature per second [$Q_{V,\mathrm{RT,ATM}}$ (m^3/s)] from Eqs. (2) and (A5) with constancy of mass-flow rate Q_W

$$Q_{V,\mathrm{RT,ATM}} = (1/P_{\mathrm{ATM}})(T_{\mathrm{R.T.}}/T)Q \tag{A7}$$

where $T_{\mathrm{R.T.}}$ (K) is the room temperature and P_{ATM} (Pa) is the atmospheric pressure.

Appendix B: Crack-Opening Displacements Based on Two-Dimensional Shear-Lag Analysis

Shear-lag analysis for calculation of crack-opening displacements in $(0_n/90_m)_S$ cross-ply laminates subjected to in-plane tensile stresses σ_x and σ_y is formulated based on the assumption of deformations of cracked layers.[9] In this analysis the cross-ply laminates are assumed to have symmetric stacking sequence such as $(0_n/90_m)_S$. The x and y axes coincide with the 0- and 90-deg directions, respectively, and the z axis is the direction of the ply thickness. The ply thicknesses of 0- and 90-deg layers are denoted as $2t_0$ and t_{90}, respectively, and the matrix cracks in the laminate are assumed to be uniformly spaced along the x and y directions at Dx and Dy intervals as shown in Fig. B1.

Crack-opening displacements are considered to be of quadratic functions in the thickness direction, and x- and y-directional displacements u and v in the laminate are assumed to be

$$u = u^{90} + \left(z^2/t_{90}^2\right)(u^0 - u^{90}), \qquad (-t_{90} \le z \le +t_{90}) \tag{B1}$$

$$v = v^{90}, \qquad (-t_{90} \le z \le +t_{90}) \tag{B2}$$

$$u = u^{90}, \qquad (t_{90} \le |z| \le t_{90} + t_0) \tag{B3}$$

$$v = v^0 + \left[(z - t_0 - t_{90})^2/t_0^2\right](v^0 - v^{90}), \qquad (t_{90} \le |z| \le t_{90} + t_0) \tag{B4}$$

where u^0, v^{90}, u^{90}, and v^0 are functions of coordinates x and y.

The shearing stresses at 0/90 deg interface τ_{xz}^{90i} and τ_{yz}^{90i} are derived from Eqs. (B1–B4), with assumptions of $\partial w/\partial x \approx 0$ and $\partial w/\partial y \approx 0$ (w is z-directional displacement), as

$$\tau_{xz}^{90i} = (2G_{23}/t_{90})(u^0 - u^{90}) \tag{B5}$$

$$\tau_{yz}^{0i} = (2G_{23}/t_0)(v^0 - v^{90}) \tag{B6}$$

where G_{23} is the out-of-plane shear modulus of a ply.

Solving the equilibrium equations together with Eqs. (B5) and (B6), the constitutive equations and boundary conditions, the average stresses in 0-deg layer σ_x^0 and σ_y^0 are obtained as follows:

$$\sigma_x^0 = A_x \cosh(R_x x) + B_x \cosh(R_y y) + K_x \tag{B7}$$

$$\sigma_y^0 = A_y \cosh(R_x x) + B_y \cosh(R_y y) + K_y \tag{B8}$$

where A_i, B_i, R_i, and K_i $(i = x, y)$ depend on geometrical and damage parameters, elastic constants, applied stresses, and initial strains. A_i, B_i, and K_i $(i = x, y)$ are linear functions of applied stresses and initial strains, and thus the average stresses σ_x^0 and σ_y^0 are linear functions of applied stresses and initial strains. Similarly average stresses in 90-deg layer σ_x^{90} and σ_y^{90} have the same linearity.

Crack-opening displacements in Eqs. (B1–B4) are also the linear functions of applied stresses and initial strains as the strains are linear combinations of stresses, which are linear functions of applied stresses and initial strains. Then average crack-opening displacements $\overline{\Delta_0}$ and $\overline{\Delta_{90}}$, which are calculated from quadratic crack-opening displacements, can be expressed as x- and y-directional

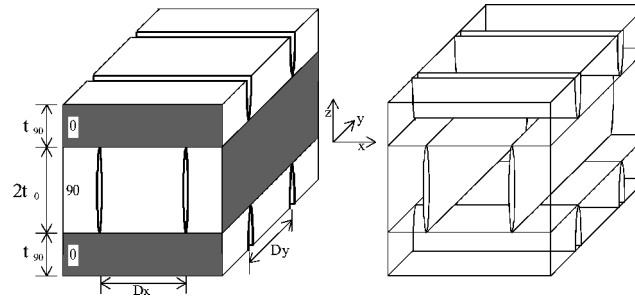

Fig. B1 Crack geometry used for modeling in cross-ply laminate.

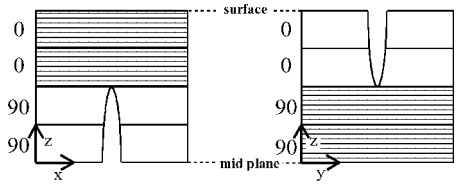

Fig. B2 Symmetrical geometry in $(0/0/90/90)_S$ cross-ply laminate.

average stresses ($\overline{\sigma_x}$ and $\overline{\sigma_x}$) and longitudinal and transverse thermal strains (ε_{10} and ε_{20}) of the laminate as follows:

$$\overline{\Delta_i}(\overline{\sigma_x}, \overline{\sigma_y}, \varepsilon_{10}, \varepsilon_{20}) = H_{iA}\overline{\sigma_x} + H_{iB}\overline{\sigma_y} + I_{iA}\varepsilon_{10} + I_{iB}\varepsilon_{20} \quad (i = 0, 90) \quad \text{(B9)}$$

where H_{ij} and I_{ij} $(j = A, B)$ are constants.

In particular, average crack-opening displacements $\overline{\Delta_0}$ and $\overline{\Delta_{90}}$ are the functions of applied stresses and temperature difference $(T - T_0)$ when coefficients of thermal expansion are constant:

$$\overline{\Delta_i}(\overline{\sigma_x}, \overline{\sigma_y}, T) = H_{iA}\overline{\sigma_x} + H_{iB}\overline{\sigma_y} + I_i(T - T_0) \quad (i = 0, 90) \quad \text{(B10)}$$

where I_i is a constant.

In this paper the preceding analysis was applied to the $(0/0/90/90)_S$ cross-ply laminates. Coefficients in Eq. (B9) in the case that crack spacings in 0- and 90-deg layers are equal or adequately large have the following relationships because of the symmetrical conditions of material constants and geometry of laminates as shown in Fig. B2:

$$H_{0A} = H_{90B}, \qquad H_{0B} = H_{90A}, \qquad I_{0A} = I_{90A}, \qquad I_{0B} = I_{90B}$$

Then average crack-opening displacements in 0- and 90-deg layers satisfy the following equation:

$$\overline{\Delta_0}(\sigma_1, \sigma_2, \varepsilon_{10}, \varepsilon_{20}) = \overline{\Delta_{90}}(\sigma_2, \sigma_1, \varepsilon_{10}, \varepsilon_{20}) \quad \text{(B11)}$$

In Eq. (B11) crack-opening displacements are symmetric with respect to biaxial stresses for the laminate used in this paper.

Acknowledgments

The authors acknowledge Yoichi Hayashi from the Tokyo Business Service and Takashi Ishikawa from the National Aerospace Laboratory of Japan for their invaluable contributions to this research.

References

[1]Aoki, T., Ishikawa, T., Kumazawa, H., and Morino, Y., "Cryogenic Mechanical Properties of CF/Polymer Composite for Tanks of Reusable Rockets," *Advanced Composite Materials*, Vol. 10, 2001, pp. 349–356.

[2]Schoeppner, G. A., Kim, R., and Donaldson, S. L., "Steady State Cracking of PMCS at Cryogenic Temperatures," AIAA Paper 2001-1216, April 2001.

[3]"Final Report of the X-33 Liquid Hydrogen Tank Test Investigation Team," NASA Marshal Space Flight Center, May 2000.

[4]Okada, T., Nishijima, S., Fujioka, K., and Kuraoka, Y., "Gas Permeation and Performance of an FRP Cryostat," *Advances in Cryogenic Engineering*, Vol. 34, 1988, pp. 17–24.

[5]Disdier, S., Rey, J. M., Pailler, P., and Bunsell, A. R., "Helium Permeation in Composite Materials for Cryogenic Application," *Cryogenics*, Vol. 38, 1998, pp. 135–142.

[6]Rivers, H. K., Sikora, J. G., and Sankaran, S. N., "Detection of Hydrogen Leakage in a Composite Sandwich Structure at Cryogenic Temperature," *Journal of Spacecraft and Rockets*, Vol. 39, 2002, pp. 452–459.

[7]Robinson, M. J., Eichinger, J. D., and Johnson, S. E., "Hydrogen Permeability Requirements and Testing for Reusable Launch Vehicle Tanks," AIAA Paper 2002-1418, April 2002.

[8]Holkeboer, D. H., Pagano, F., Jones, D. W., and Santeler, D. J., *Vacuum Engineering*, Boston Technical Publishers, Boston, 1967, pp. 23–28, 83–116.

[9]Henaff-Gardin, C., Lafarie-Frenot, M. C., and Gamby, D., "Doubly Periodic Matrix Cracking in Composite Laminates Part 1: General In-Plane Loading," *Composite Structures*, Vol. 36, 1996, pp. 113–130.

K. N. Shivakumar
Associate Editor